UNIVERSITY OF LEEDS

This is a repository copy of *Robust iterative feedback tuning control of a compliant rehabilitation robot for repetitive ankle training*.

White Rose Research Online URL for this paper:
http://eprints.whiterose.ac.uk/125848/

Version: Accepted Version

Article:
Meng, W orcid.org/0000-0003-0209-8753, Xie, SQ, Liu, Q et al. (2 more authors) (2017) Robust iterative feedback tuning control of a compliant rehabilitation robot for repetitive ankle training. IEEE/ASME Transactions on Mechatronics, 22 (1). pp. 173-184. ISSN 1083-4435

https://doi.org/10.1109/TMECH.2016.2618771

(c) 2017 IEEE. Personal use of this material is permitted. Permission from IEEE must be obtained for all other uses, in any current or future media, including reprinting/republishing this material for advertising or promotional purposes, creating new collective works, for resale or redistribution to servers or lists, or reuse of any copyrighted component of this work in other works

Reuse
Items deposited in White Rose Research Online are protected by copyright, with all rights reserved unless indicated otherwise. They may be downloaded and/or printed for private study, or other acts as permitted by national copyright laws. The publisher or other rights holders may allow further reproduction and re-use of the full text version. This is indicated by the licence information on the White Rose Research Online record for the item.

Takedown
If you consider content in White Rose Research Online to be in breach of UK law, please notify us by emailing eprints@whiterose.ac.uk including the URL of the record and the reason for the withdrawal request.

White Rose university consortium
Universities of Leeds, Sheffield & York

eprints@whiterose.ac.uk
https://eprints.whiterose.ac.uk/

Robust Iterative Feedback Tuning Control of a Compliant Rehabilitation Robot for Repetitive Ankle Training

Wei Meng, Sheng Q. Xie*, *Senior Member, IEEE*, Quan Liu, Charles Z. Lu, and Qingsong Ai

***Abstract*—Robot-assisted rehabilitation offers benefits such as repetitive, intensive and task specific training as compared to traditional manual manipulation performed by physiotherapists. In this paper, a robust iterative feedback tuning (IFT) technique for repetitive training control of a compliant parallel ankle rehabilitation robot is presented. The robot employs four parallel intrinsically compliant pneumatic muscle actuators that mimic skeletal muscles for ankle's motion training. A multiple degrees-of-freedom normalised IFT technique is proposed to increase the controller robustness by obtaining an optimal value for the weighting factor and offering a method with learning capacity to achieve an optimum of the controller parameters. Experiments with human participants were conducted to investigate the robustness as well as to validate the performance of the proposed IFT technique. Results show that the normalised IFT scheme will achieve a better and better tracking performance during the robot repetitive control and provides more robustness to the system by adapting to various situations in robotic rehabilitation.**

***Index Terms*—Iterative feedback tuning, normalised criterion, ankle rehabilitation robot, repetitive training**

I. INTRODUCTION

Rehabilitation using robots has several distinct advantages as compared to traditional manual manipulation. By using robotic devices, it is possible to perform the required training tasks repeatedly and accurately without requiring heavy physical demands from physiotherapists [1]. Ankle joint is one of the most complicated structures in human skeleton and plays a crucial role in balancing human body during walking and ambulation [2]. In terms of ankle rehabilitation, as parallel robots are more accurate than comparable serial manipulators and can also generate higher force and torque, a range of parallel platform-based devices have been developed [3]. Rutgers Ankle is a typical parallel ankle rehabilitation robot based on Stewart platform [4]. A parallel ankle robot ARBOT was also designed by Saglia et al. [5]. However, the existing platform-based robots are usually actuated from the bottom and one major shortcoming is that their end-effectors are typically constrained about a centre of rotation which does not coincide with the actual human ankle joint [6]. Thereby the shank's position will not be consistent during the operation, and the orientation of the robotic platform is thus unlikely to be the same as the actual rotation of ankle joint. Meanwhile, a majority of existing devices utilise rigid actuators such as electric motors or cylinders which are not back-driveable [7]. As a result of this, the human interaction environment is not fully compliant during operation of the devices.

To overcome the limitations, a novel ankle rehabilitation platform was developed by the University of Auckland to improve on existing ankle rehabilitation solutions. The design utilised a parallel kinematic structure where the power is actuated from the top and is capable of fixing the ankle joint centre of rotation by using a wearable structure [8]. Pneumatic muscle actuators (PMAs) possessing advantages in terms of soft, light weight, and high power/weight ratio were adopted to guarantee the intrinsic compliance of the robot. However, PMAs exhibit highly nonlinear and time varying features, and it is difficult to obtain the accurate dynamic model of such actuator [9]. A major limitation of model-based approach is its sensitivity to modelling accuracy of the controlled objective, it requires the system designer to have an intimate knowledge of the target. Considering the controlled objective in this study, the PMAs-driven robot expands with patient's dynamics will become more complex, thus an accurate rehabilitation robot model is hardly available in practice. Even if an accurate model can be obtained, the order of resulting controller is often too high to be suitable for practical usage [10]. In comparison, by using model-free data-driven theory, where the controller is designed directly using online data without explicit or implicit information of the underlying model, the shortcomings of model-based method can be mitigated [11].

For rehabilitation recovery, clinical studies have shown that repetitive, intensive as well as task specific rehabilitation programmes can contribute significantly to the effectiveness of treatment [12]. The repetitive nature of robot-assisted therapy provides a good opportunity for iterative learning control (ILC) techniques [13]. ILC is able to learn from data recorded from the previous trials and update the controller to optimise its

Wei Meng is with the Department of Mechanical Engineering, University of Auckland, Auckland, 1010 New Zealand and also with School of Information Engineering, Wuhan University of Technology, Wuhan, 430070 China (e-mail: wmen386@aucklanduni.ac.nz or weimeng@whut.edu.cn).

Sheng Q. Xie and Charles Z. Lu are with the Department of Mechanical Engineering, University of Auckland, Auckland, 1010 New Zealand (e-mail: s.xie@auckland.ac.nz; zlu013@aucklanduni.ac.nz).

Quan Liu and Qingsong Ai are with the School of Information Engineering, and the Key Laboratory of Fiber Optic Sensing Technology and Information Processing, Wuhan University of Technology, Wuhan, 430070 China (e-mail: quanliu@whut.edu.cn; qingsongai@whut.edu.cn).

performance [14]. As mentioned above, the device utilises a novel type of pneumatic powered actuator, and the speed and range of patient's recovery can lead to significant changes to the model of the rehabilitation robot, all of which indicate that a model-based method is not suitable, and a robust model-free method will be a prime candidate. Iterative feedback tuning (IFT) is a model-free data-driven learning method [15]. Further, IFT is very much suitable for repeated rehabilitation trajectories due to the requirement of specially designed experiments. On the other hand, IFT as compared to traditional control systems has the advantage where it can be auto-tuned only depending on the input and output data collected from the experiments, which does not contain any model information about the controlled plant. This allows the system to be highly robust to uncertainties [16, 17].

There have been some interesting cases for the application of IFT in various industrial fields, such as DC-servo control, robotic arm and mass spring system, etc., due to its superior model-free automatic tuning capacity [17-21]. However, the use of iterative feedback learning control in rehabilitation has not been well-explored [22]. The most prominent case for application of ILC on rehabilitation devices is to control the value of functional electrical stimulation (FES) for upper limb therapy as presented in [23, 24], in which ILC was worked as a kind of "high-level" controller to adjust the amount of FES for upper limb. Few other previous researches invoke the use of ILC on rehabilitation platforms. In [25], a form of iterative learning control was implemented on the Lokomat robot to synchronise the leg and treadmill movements. A PID plus iterative learning-based feed forward controller was proposed on an upper extremity therapy robot for repetitive task training [13]. As for the iterative feedback tuning technique, there is no reported literature on the specific combination of IFT and rehabilitation devices, also no IFT instances on PMAs-driven equipment. By transferring the idea of IFT to rehabilitation robotics, we believe that the robot controller can also improve its performance from repetitive trials.

In rehabilitation environment, there is often an external disturbance from the patient during the training and this will lead to significant changes to the control parameters of the robot used. Therefore, robust control system implementation is one major difficult task and it is even harder to enhance the robustness during long time repetitive training. Hussain et al. utilised a charting-free robust variable structure controller for the designed robotic gait orthosis [26]. Xu et al. proposed an evolutionary dynamic recurrent fuzzy neural network to provide more robustness for upper limb rehabilitation [27]. One shortcoming of these methods if applying them to our system is that the dynamic modelling of pneumatic muscles and robot behaviour would bring heavy computation burden to the control system, and it is also difficult to model the patient's arbitrary activities. One advantage of IFT technique is its ability to learn from repeating scenarios and optimise the controller parameters without knowledge of the actual system, which guarantees the inherent robustness of such a method [15, 17, 28]. To obtain a more robust control system, the design criterion or objective function of IFT must be taken into account. Introduce a plenty function to the input signal for certain restrictions is a typical approach to increase the system robustness, such as the studies in [17] and [28]. However, in rehabilitation scenarios the robot system will have various desired and actual output, error, as well as control input signal, especially when treat patients in different recovery stages and with different active intentions. The robustness problem of IFT controller should be investigated further. We will propose a novel robust IFT controller to make the controller system agnostic and meaningful across different situations.

According to the authors' best knowledge, IFT control of a rehabilitation robot has not been reported in the literature. In this paper, a normalised IFT (NIFT) technique is applied for the repetitive training control of a flexible ankle rehabilitation robot actuated by PMAs. A novel multiple degrees-of-freedom (DOFs) IFT method with normalised criterion is proposed to improve the robustness under varying training conditions. The rest of this paper is organised as follows: Section II demonstrates the details of the compliant ankle rehabilitation robot. In Section III, methodology of the proposed multiple DOFs normalised IFT method is presented. Experiments including comparison test and human participants test were conducted in Section IV, followed by the discussion in Section V. The conclusion is drawn in Section VI.

II. Compliant Ankle Rehabilitation Robot

We had developed a novel ankle rehabilitation platform, with the new prototype shown in Fig. 1. This robot is actuated by four parallel links to realise three rotational DOFs of the end-effector for ankle dorsiflexion/plantarflexion, inversion/eversion, and adduction/abduction, respectively. Each joint is actuated using a pneumatic muscle actuator from FESTO™ (FESTO DMSP-20-400N) in order to guarantee the intrinsic compliance of the robot during operation. It has a stroke length of 100mm, a maximum force of over 5000N, and an internal diameter of 20mm. Each pneumatic muscle actuator is controlled by a proportional pressure regulator. The end-effector is a three-link serial manipulator with three rotational DOFs, in which three magnetic rotary encoders are installed to provide measurements of angular positions of the robot in Euler X, Y and Z axes. Additionally, a six-axis load cell is mounted between the robot end-effector and a human foot to measure the human robot interaction force and torque. For the control system hardware, a National Instruments embedded controller (NI Compact RIO-9022) is adopted for real-time control. The control system now runs on a host PC using LabVIEW™, with the communication between the PC and the embedded solution performed using the TCP/IP protocol.

In order to control the robot end-effector to track a predefined trajectory for ankle movement training, the robot kinematic model must be studied. Inverse kinematics of a robot describes the translation of the end-effector orientation to the length of the active links, which is essential for any form of robot control. Fig. 2 presents the robotic kinematic geometry of the developed parallel ankle rehabilitation robot. The fixed coordinate frame is denoted by O_f and the moving one is

denoted by O_m. Connection points on the fixed and moving platforms are denoted by p_i^f and p_i^m, respectively, and their position vectors P_i^f and P_i^m are defined in (1) as well as the position vector $\overrightarrow{O_f O_m}$, where H is the centre distance between the fixed platform and the moving end-effector. A table of all variables can be found in the Nomenclature.

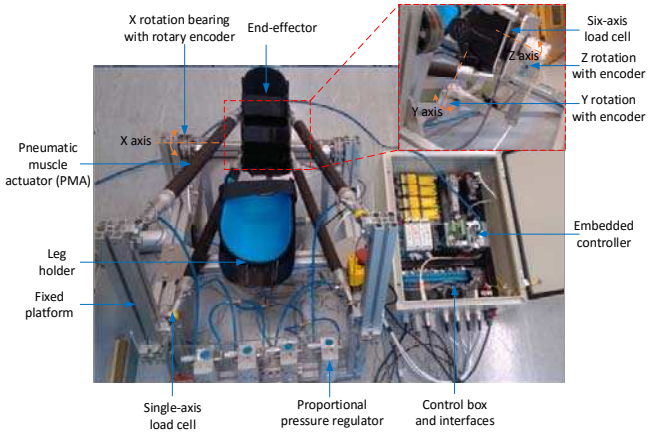

Fig. 1. Prototype of the compliant parallel ankle rehabilitation robot.

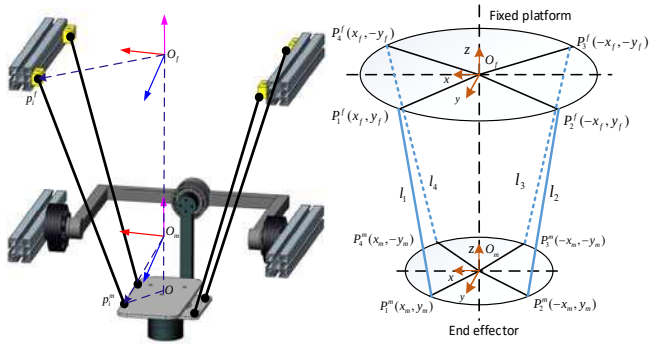

Fig. 2. Kinematic structure of the parallel ankle rehabilitation robot.

As shown in Fig. 2, by defining the connection points and a rotating coordinate system, the vector of each active link L_i can be calculated. The position vector L_i of the link is described in (2), where the rotational transformation matrix of the end-effector with respect to the fixed platform is denoted by matrix R_m^f using a sequence of $\theta_X, \theta_Y, \theta_Z$. The link length is expressed by l_i in (3), where C is the *cosine* function, S is the *sine* function, and the subscripts represent corresponding Euler angles, for example, $C_x = cos\theta_X, S_y = sin\theta_Y$.

$$\begin{cases} P_i^f = [x_i^f \quad y_i^f \quad 0]^T \\ P_i^m = [x_i^m \quad y_i^m \quad 0]^T \\ O = \overrightarrow{O_f O_m} = [0 \quad 0 \quad -H]^T \end{cases} \tag{1}$$

$$L_i = O_f + R_m^f P_i^m - P_i^f \tag{2}$$

$$l_i = \sqrt{L_i{}^T L_i} \tag{3}$$

$$R_m^f = \begin{bmatrix} C_z C_y & -S_z C_x + C_z S_y S_x & S_z S_x + C_z S_y C_x \\ S_z C_y & C_z C_x + S_z S_y S_x & -C_z S_x + S_z S_y C_x \\ -S_y & C_y S_x & C_y C_x \end{bmatrix} \tag{4}$$

III. Multi-DOF NIFT Control System

As the ankle rehabilitation robot has multiple actuators to be controlled, the implementation of multiple instances of the IFT technique is explored. The base control structure is presented in Fig. 3, where inverse kinematics is used to obtain the joint space trajectory $l_i, i = 1,2,3,4$ for each actuator. The reference and actual position of each link are evaluated from the desired orientation $\theta_{d,XYZ}$ and the measured end-effector orientation θ_{XYZ} respectively by using inverse kinematics. These actuators are then controlled individually using a PID controller with the parameter vector being tuned by the IFT technique. In the control structure, the same set of starting parameters of $\rho = [K_P \quad K_I \quad K_D]^T$ was applied to all four controllers. The outer control loop regulates the angular position, and each of the inner control loops regulates air pressure of each PMA. The PMA model is used to convert the control signal u_i into air pressure p_i for each proportional regulator.

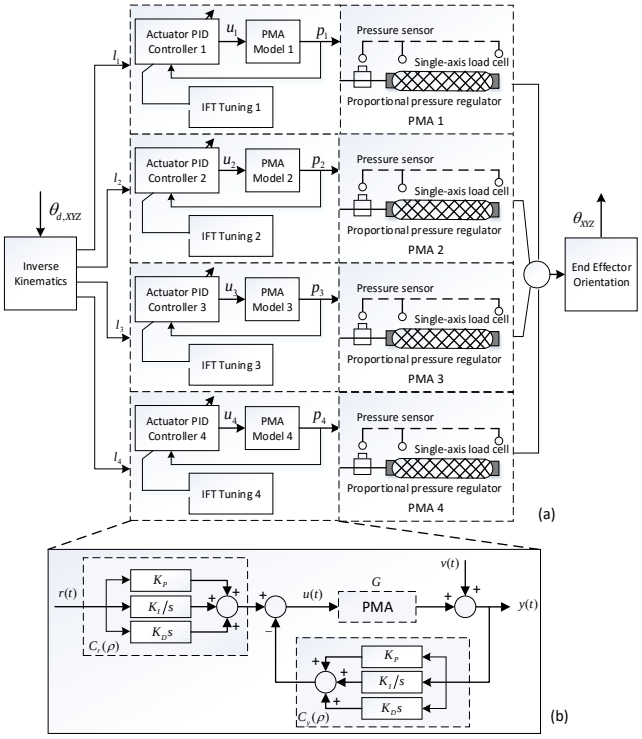

Fig. 3. Control system of the ankle rehabilitation robot. (a) Structure of the multiple DOFs IFT. (b) Diagram of the controller for each PMA.

A. IFT Tuning of PID parameters on PMA

Each pneumatic muscle is controlled individually using a standard PID controller, and for IFT tuned PID controller, as suggested by [29], it must be considered as a 2-DOF controller with common parameters. A block diagram of the controller in the form $C(\rho) = [C_r(\rho), \ C_y(\rho)]$ is shown in Fig. 3 (b), where $C_r(\rho)$ and $C_y(\rho)$ sharing the same parameters both together constitute the PID controller. The PMA is considered as an unknown system G, and r the reference input, u the controller output, y the response output, v the unmeasurable disturbance. The parameters for C_r and C_y are collected and optimised in a vector of controller parameters: $\rho = [K_P \quad K_I \quad K_D]^T$.

Considering the controller shown in Fig. 3 (b), the system

response can be expressed by using (5).

$$y_t(\rho) = \frac{C_r(\rho)G}{1 + C_y(\rho)G} r_t + \frac{1}{1 + C_y(\rho)G} v_t = T_0 r_t + S_0 v_t \quad (5)$$

The objective for an iterative learning control is to generate a sequence of appropriate control inputs $u_t(i)$ to drive the system output $y_t(i)$ approaches the reference trajectory y_d, for iteration i. Each iteration of control input generation should take the output $y_t(i)$ closer to the reference trajectory by the IFT algorithm. Details of the general IFT algorithm can be found in [29]. The used design criterion $J(\rho)$ takes into account both the error response as well as the controller input magnitude. λ is a predetermined weighting factor between the two cost function component variables, and is usually obtained empirically through trial and error. More discussion on the selection of λ will be presented in next section.

$$J(\rho) = \frac{1}{2N}\left(\sum_{t=1}^{N} \tilde{y}_t(\rho)^2 + \lambda \sum_{t=1}^{N} u_t(\rho)^2 \right) \quad (6)$$

Here ρ is a vector of process parameters to be optimised, $\tilde{y}_t(\rho)$ is the error between the actual output and the desired output signal ($\tilde{y}_t(\rho) = y_t(\rho) - y_d$, so $\frac{\partial \tilde{y}_t(\rho)}{\partial \rho} = \frac{\partial y_t(\rho)}{\partial \rho}$), and N is the total number of samples collected. The optimised controller parameter vector ρ^* is defined as shown in (7).

$$\rho^* = \arg\min_{\rho} J(\rho) \quad (7)$$

The partial derivative of $\tilde{y}_t(\rho)$ and $u_t(\rho)$ with respect to the controller parameters ρ is:

$$\frac{\partial y_t}{\partial \rho}(\rho) = \frac{1}{C_r(\rho)}\left[\frac{\partial C_r}{\partial \rho}(\rho) T_0 r_t - \frac{\partial C_y}{\partial \rho}(\rho) T_0 y_t \right] \quad (8)$$

$$\frac{\partial u_t}{\partial \rho}(\rho) = S_0 \left[\frac{\partial C_r}{\partial \rho}(\rho) r_t - \frac{\partial C_y}{\partial \rho}(\rho) y_t \right] \quad (9)$$

The partial derivatives $\frac{\partial y_t(\rho_i)}{\partial \rho}$ and $\frac{\partial u_t(\rho_i)}{\partial \rho}$ can be obtained by performing actual experiments on the system. Normally, three experiments are required to complete each iteration of the optimisation process. First, a reference signal is applied to the closed-loop system as input and the output data is recorded. Second, the output from the first experiment is re-applied to the system as the reference input. A third experiment is performed where the first test signal is used as the reference [30]. The outputs from the second and the third experiment will be utilised to calculate the gradient of the controller parameters. As illustrated by Eq. (10), this is done to ensure that the data from the second and third experiments are independent of each other in order to reduce bias.

$$\begin{cases} r_i^1 = r & u_t^1 = S_0(C_r r - C_y v_i^1) & y_t^1 = T_0 r + S_0 v_i^1 \\ r_i^2 = y^1 & u_t^2 = S_0(C_r y^1 - C_y v_i^2) & y_t^2 = T_0 y^1 + S_0 v_i^2 \\ r_i^3 = r & u_t^3 = S_0(C_r r - C_y v_i^3) & y_t^3 = T_0 r + S_0 v_i^3 \end{cases} \quad (10)$$

Here v_i^j are disturbances come from different experiments and thus are mutually independent. Then, the unbiased estimate of the partial derivatives can be achieved by:

$$est\left[\frac{\partial y_t}{\partial \rho}(\rho)\right] = \frac{1}{C_r(\rho)}\left[\frac{\partial C_r}{\partial \rho}(\rho) y_t^3 - \frac{\partial C_y}{\partial \rho}(\rho) y_t^2 \right] \quad (11)$$

$$est\left[\frac{\partial u_t}{\partial \rho}(\rho)\right] = \frac{1}{C_r(\rho)}\left[\frac{\partial C_r}{\partial \rho}(\rho) u_t^3 - \frac{\partial C_y}{\partial \rho}(\rho) u_t^2 \right] \quad (12)$$

As $C_r(\rho)$ and $C_y(\rho)$ are PID controllers with the same parameter vector $\rho = [K_P \quad K_I \quad K_D]^T$, transfer function of PID controller is: $K_P + K_I/s + K_d s$. For discrete system:

$$C_r(\rho) = C_y(\rho) = \frac{(K_P T + K_I T^2 + K_D) z^2 - (K_P T + 2K_D) z + K_D}{Tz^2 - Tz} \quad (13)$$

$$\frac{\partial C_y}{\partial K_P} = \frac{\partial C_r}{\partial K_P} = \frac{Tz^2 - Tz}{Tz^2 - Tz}, \quad \frac{\partial C_y}{\partial K_I} = \frac{\partial C_r}{\partial K_I} = \frac{Tz^2}{Tz^2 - Tz}, \quad \frac{\partial C_y}{\partial K_D} = \frac{\partial C_r}{\partial K_D} = \frac{z^2 - 2z + 1}{Tz^2 - Tz} \quad (14)$$

The partial derivative of y_t and u_t with respect to each controller parameter can be written as:

$$est\left[\frac{\partial y_t}{\partial \rho}(\rho)\right] = \begin{bmatrix} \frac{\partial y_t}{\partial K_P} \\ \frac{\partial y_t}{\partial K_I} \\ \frac{\partial y_t}{\partial K_D} \end{bmatrix} = \begin{bmatrix} \frac{1}{C_r(\rho)}\left[\frac{\partial C_y}{\partial K_P}(\rho)(y_t^3 - y_t^2)\right] \\ \frac{1}{C_r(\rho)}\left[\frac{\partial C_y}{\partial K_I}(\rho)(y_t^3 - y_t^2)\right] \\ \frac{1}{C_r(\rho)}\left[\frac{\partial C_y}{\partial K_D}(\rho)(-y_t^2)\right] \end{bmatrix} \quad (15)$$

$$est\left[\frac{\partial u_t}{\partial \rho}(\rho)\right] = \begin{bmatrix} \frac{\partial u_t}{\partial K_P} \\ \frac{\partial u_t}{\partial K_I} \\ \frac{\partial u_t}{\partial K_D} \end{bmatrix} = \begin{bmatrix} \frac{1}{C_r(\rho)}\left[\frac{\partial C_y}{\partial K_P}(\rho)(u_t^3 - u_t^2)\right] \\ \frac{1}{C_r(\rho)}\left[\frac{\partial C_y}{\partial K_I}(\rho)(u_t^3 - u_t^2)\right] \\ \frac{1}{C_r(\rho)}\left[\frac{\partial C_y}{\partial K_D}(\rho)(-u_t^2)\right] \end{bmatrix} \quad (16)$$

The estimated gradient of the design criterion $J(\rho)$ for the i^{th} iteration based entirely on experimental data can be constructed from the estimated partial derivatives:

$$est\left[\frac{\partial J}{\partial \rho}(\rho_i)\right] = \frac{1}{N}\sum_{t=1}^{N}\left(\tilde{y}_t(\rho_i) est\left[\frac{\partial y_t}{\partial \rho}(\rho_i)\right] + \lambda u_t(\rho_i) est\left[\frac{\partial u_t}{\partial \rho}(\rho_i)\right] \right) \quad (17)$$

The next iterate $\rho_{i+1} = [K_P^{i+1} \quad K_I^{i+1} \quad K_D^{i+1}]^T$ is calculated by using the Gauss-Newton optimisation algorithm, based on the gradient of $J(\rho)$ and previous $\rho_i = [K_P^i \quad K_I^i \quad K_D^i]^T$.

$$\rho_{i+1} = \rho_i - \gamma_i R_i^{-1} est\left[\frac{\partial J}{\partial \rho}(\rho_i)\right] \quad (18)$$

where γ_i is a positive value to indicate the step size. R_i is a matrix to imply the optimised search direction, here a positive Gauss-Newton approximation to the Hessian matrix is applied:

$$R_i = \frac{1}{N}\sum_{t=1}^{N}\left(est\left[\frac{\partial y_t}{\partial \rho}(\rho_i)\right] est\left[\frac{\partial y_t}{\partial \rho}(\rho_i)\right]^T + \lambda est\left[\frac{\partial u_t}{\partial \rho}(\rho_i)\right] est\left[\frac{\partial u_t}{\partial \rho}(\rho_i)\right]^T \right) \quad (19)$$

It is essential to select a proper step size for IFT to maintain the balance between convergence and stability of the IFT algorithm. Firstly, the step size must obey some constraints so that the design criterion can converge to a local minimum soon [29]. Secondly, the step size must be chosen to make the closed-loop system maintain stable [31]. Usually a step size with constraint $0 < \gamma_i \leq 1$ will be applied [28]. As suggested by [21], if the step size is set small enough and the dataset is relatively large, the convergence of IFT algorithm can be ensured. In practice, the step size for each controller will need to be defined empirically, often through trial and error.

B. Normalised design criterion for IFT

The performance of the IFT process can be influenced by several factors. In order to determine an optimal value of λ, it is important to consider the relative magnitudes of each variable in the design criterion $J(\rho)$. Different systems will have variable desired and actual output, error, as well as control signal. When considering the combination of $\tilde{y}_t(\rho)$ and $u_t(\rho)$, the λ value obtained from trial and error will contain the properties specific to the system being tuned. There needs to be a method to remove the system properties from λ, as in making weighting factor λ normalised so that it can be comparable and agnostic across different systems [32]. Eq. (20) proposes a normalised design criterion, where a normalising factor K_n is introduced, and λ_n replaces λ to be the weighting factor that remains meaningful.

$$J_n(\rho) = \frac{1}{2N}\sum_{t=1}^{N}(\tilde{y}_t(\rho)^2 + \lambda_n K_n u_t(\rho)^2) \tag{20}$$

where the normalising coefficient K_n is determined by:

$$K_n = \frac{y_{d,max} - y_{d,min}}{u_{t,max} - u_{t,min}} \tag{21}$$

where $y_{d,max}, y_{d,min}, u_{t,max}$ and $u_{t,min}$ are the maximum and minimum value in the desired output and the control signal, respectively. As all four values are only determined at the end of each optimisation iteration, all data points are taken into account so the normalisation process is a fair representation of the current iteration. The normalised design criterion for IFT ensures that the value of λ_n stays meaningful across different tuning iterations [30]. With normalised design criterion, it becomes possible to determine sets of λ_n values that represent the optimal range for IFT tuning for various situations.

The estimated gradient of the normalised design criterion $J_n(\rho)$ for the i^{th} iteration can be then constructed by using (22) and the Gauss-Newton Hessian matrix $R_{n,i}$ becomes (23):

$$\begin{aligned} est\left[\frac{\partial J_n}{\partial \rho}(\rho_i)\right] = \frac{1}{N}\sum_{t=1}^{N}\Bigg(&\tilde{y}_t(\rho_i) est\left[\frac{\partial y_t}{\partial \rho}(\rho_i)\right] \\ &+ \lambda_n K_n u_t(\rho_i) est\left[\frac{\partial u_t}{\partial \rho}(\rho_i)\right]\Bigg) \end{aligned} \tag{22}$$

$$\begin{aligned} R_{n,i} = \frac{1}{N}\sum_{t=1}^{N}\Bigg(&est\left[\frac{\partial y_t}{\partial \rho}(\rho_i)\right] est\left[\frac{\partial y_t}{\partial \rho}(\rho_i)\right]^T \\ &+ \lambda_n K_n est\left[\frac{\partial u_t}{\partial \rho}(\rho_i)\right] est\left[\frac{\partial u_t}{\partial \rho}(\rho_i)\right]^T\Bigg) \end{aligned} \tag{23}$$

Therefore, the key to the iterative feedback tuning method is the iterative computation of $\frac{\partial J_n}{\partial \rho}(\rho)$ and $R_{n,i}$ from experiment results. As long as $y_t(\rho_i)$ and $u_t(\rho_i)$ and the gradients $\frac{\partial y_t}{\partial \rho}(\rho_i)$ and $\frac{\partial u_t}{\partial \rho}(\rho_i)$ are obtained, the $\frac{\partial J_n}{\partial \rho}(\rho_i)$ and $R_{n,i}$ can be estimated by the introduction of λ_n and K_n. Then the controller parameters can be updated accordingly:

$$\rho_{i+1} = \rho_i - \gamma_i R_{n,i}^{-1} est\left[\frac{\partial J_n}{\partial \rho}(\rho_i)\right] \tag{24}$$

To summarise, the procedure of normalised IFT algorithm is: (i) Choose the starting controller parameters ρ_0 and select the normalized design criterion $J_n(\rho)$; (ii) Perform three experiments $r_i^1 = r,\ r_i^2 = y^1,\ r_i^3 = r$; (iii) Estimate partial derivatives $\frac{\partial y_t}{\partial \rho}(\rho_i)$ and $\frac{\partial u_t}{\partial \rho}(\rho_i)$; (iv) Evaluate the gradient of criterion $\frac{\partial J_n}{\partial \rho}(\rho_i)$ and Hessian matrix $R_{n,i}$; (v) Obtain the new controller parameters ρ_{i+1}; and (vi) Evaluate the criterion $J_n(\rho)$ and check the performance, if stop criterion reached go to (vii) finish, otherwise go to (ii) for next iteration loop.

C. Convergence and robustness aspects

Convergence property of standard IFT has been analysed in [29] and [16], here we study the normalised IFT method. The convergence conditions as stated in [33] are: (1) the estimated gradient of the objective function is unbiased; (2) the step size sequence converges to zero but not too fast.

For Condition (1), the unbiased gradient estimate is the key property of IFT. In this study we use three specially designed experiments to generate the gradient based descent direction, which can obtain unbiased gradient estimates without the use of parametric models [28]. From Eq. (8)-(10), the following expression of derivatives $\frac{\partial y_t}{\partial \rho}(\rho)$ and $\frac{\partial u_t}{\partial \rho}(\rho)$ can be derived:

$$\begin{aligned} \frac{\partial y_t}{\partial \rho}(\rho) = &\frac{1}{C_r(\rho)}\left[\frac{\partial C_r}{\partial \rho}(\rho) y_t^3 - \frac{\partial C_y}{\partial \rho}(\rho) y_t^2\right] \\ &+ \frac{S_0}{C_r(\rho)}\left[\frac{\partial C_y}{\partial \rho}(\rho) v_i^2 - \frac{\partial C_r}{\partial \rho}(\rho) v_i^3\right] \end{aligned} \tag{25}$$

$$\begin{aligned} \frac{\partial u_t}{\partial \rho}(\rho) = &\frac{1}{C_r(\rho)}\left[\frac{\partial C_r}{\partial \rho}(\rho) u_t^3 - \frac{\partial C_y}{\partial \rho}(\rho) u_t^2\right] \\ &+ \frac{S_0 C_y}{C_r(\rho)}\left[\frac{\partial C_r}{\partial \rho}(\rho) v_i^3 - \frac{\partial C_y}{\partial \rho}(\rho) v_i^2\right] \end{aligned} \tag{26}$$

As v_i^2 and v_i^3 are mutually independent bounded stochastic noises of the same system, the equations (11) and (12) are the unbiased estimate of $\frac{\partial y_t}{\partial \rho}(\rho)$ and $\frac{\partial u_t}{\partial \rho}(\rho)$. Thus, the estimated gradient of the normalised objective function $J_n(\rho)$ is also unbiased, as illustrated by Eq. (22).

For Condition (2), the usual conditions for convergence can be guaranteed for the choice of γ_i:

$$\sum_{i=1}^{\infty}\gamma_i = \infty, \qquad \sum_{i=1}^{\infty}\gamma_i^2 < \infty \tag{27}$$

This condition is fulfilled e.g. by having $\gamma_i = a/i$, where a is a certain positive constant. However, this requirement may have a slow convergence rate. Though the matrix R_i that determines the update direction does not influence the IFT's convergence ability, as stated in [17], Gauss-Newton direction

is a desirable choice to speed up the convergence rate. So, the Gauss-Newton optimisation with $0 < \gamma \leq 1$ is used in this study to guarantee the algorithm convergence, which has also been suggested by [31]. By fulfilling these two conditions, the designed IFT is able to coverage to a stationary point soon.

Robustness property of the designed IFT controller can also be guaranteed. Compared to model-based procedures, which can be viewed as global approaches, IFT can be viewed as an approach where the objective function is modelled locally by using gradients. Such a method can be made robust to the uncertain systems [16]. Hjalmarsson [17] has also verified that IFT is more robust compared with model-based methods.

Furthermore, the IFT can be made more robust when the following two aspects of robustness are taken into account [17]: (1) choose the objective function (i.e. $J(\rho)$) judiciously; (2) consider iterative minimisation of the suitable function.

For Aspect (1), regarding the design objective, in general it is good to include a penalty on the input signal as well. It is also suggested by [17] that the objective function in form $J(\rho) = E[(y(\rho), u(\rho))(y(\rho), u(\rho))^T]$ would have a strong ties to robust loop-shaping. Thus, in this paper, the basic IFT objective criterion is designed as (6). To further enhance the robustness from design objective aspect, a normalised IFT design criterion $J_n(\rho)$ is proposed to eliminate the trial and error process for weighting factor selection. By normalising the input and output signals, the value of λ_n is able to stay meaningful across different tuning iterations, which is possible to make the controller be system agnostic and thus increase the robustness. It has been verified by [32] that the normalised IFT is theoretically more robust than the standard method.

For Aspect (2), as IFT method tries to estimate the gradient of the criterion, once steady minimisation of the criterion is achieved, the controller robustness can be ensured. The matrix R_i determines the update direction and is therefore crucial. As suggested by [17], Gauss-Newton update can yield close to optimal performance, which is thus applied to the NIFT algorithm in this paper, as the $R_{n,i}$ indicated by Eq. (23). Therefore, besides the inherent robustness of standard model-free data-driven IFT algorithm, the newly designed NIFT method is able to further enhance and guarantee the robustness property by taking the above two aspects into account.

IV. Experiments and Results

A. *NIFT optimisation for repetitive control*

In this experiment, IFT with normalised design criterion was used to tune the robot position control. The trajectory used was a sinusoidal waveform about the X Euler axis with an amplitude of 0.2 radians and a period of 20 seconds. The starting PID gains $\rho = [15 \quad 9 \times 10^{-3} \quad 5 \times 10^{-4}]^T$ was obtained by the commonly used Ziegler–Nichols (ZN) tuning rules, and then NIFT started tuning from the ZN sets. The step size of K_P, K_I, and K_D was empirically set as 0.1, 1×10^{-5}, and 6×10^{-6}, respectively. Usually only a few iterations are required for the IFT method to achieve a good performance [34]. Ten iterations of online optimisation were performed in this trial, with results taken directly from the tuning process.

The NIFT tuning result is shown in Fig. 4, where a positive angle in the X Euler axis denotes the dorsiflexion direction and a negative angle denotes the plantar flexion. For such a repetitive trajectory, the robot tracking performance became better and better during the ten iterations, as shown in Fig. 4 (a). It can be seen that there was a significant improvement in the performance when comparing the ZN sets (before NIFT tuning) and end of NIFT tuning results in Fig. 4 (b) and Fig. 4 (c) respectively. The errors for Euler angle axes at iteration 0 and at iteration 10 are shown in Fig. 4 (d) by the dotted and the solid line, respectively. It also provides evidence that the NIFT method was able to tune the controller towards a high-performance tracking results within several minutes. The profile of how the value of the design criterion decreased is shown in Fig. 4 (e), where there was a steady decrease in the value of $J_n(\rho)$ from over 0.02 to around 0.005.

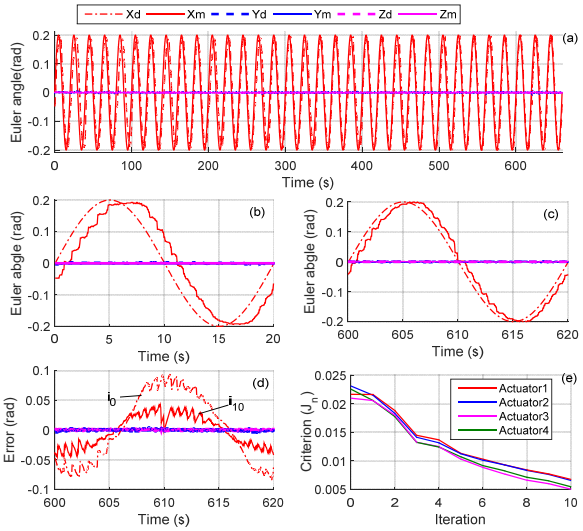

Fig. 4. Repetitive control result using normalised IFT tuning. (a) End-effector orientation during 10 iterations. (b) Tracking result before tuning (iteration 0). (c) After tuning (iteration 10). (d) End-effector errors. (e) Design criterions.

We further explored how the normalised IFT performs when compared to the standard IFT that is commonly used. The same cyclical waveform for rehabilitation trajectory was used here for online tuning. A total of four sets were tested for the PMAs-actuated robot, and ten tuning iterations were performed for each setup. A detailed comparison of the errors between the normalised and the standard IFT is presented in Table I. For normalised IFT tests, the λ_n selected was 1×10^{-4}. For the standard IFT tests, the λ value varied. The first λ value of 1×10^{-3} was adopted for the standard IFT. Obviously the result was not optimal and more control actions are needed to reach the desired trajectory. The λ value was then gradually adjusted to 1×10^{-4} and 1×10^{-5} which resulted in the system being better tuned each time. Note that for the normalised IFT design criterion, even without changing the value λ_n, the performance was even better than the standard IFT tuned with the optimal λ value. The newly normalised design criterion shows improved performance as compared to the original standard IFT design criterion.

B. *Robustness test with human participants*

To explore the adaptability of NIFT algorithm on different users and rehabilitation strategies, tests were performed on four healthy human participants aged between 20 and 30 of various gender, height and weight. The ankle movement range and active torque of each participant were assessed first by using the method presented in our previous work [35, 36], to ensure that all possessed a normal range and torque ability for the ankles tested. Each participant was first asked to adjust the seating to a correct height so the knee joint is at approximately 120 degrees when the foot is on the platform. The participant's foot was strapped to the end-effector tightly and comfortably, as indicated by Fig. 5. This trial has been approved by the University of Auckland Human Participants Ethics Committee (reference 011904). The tuning duration for each test were also set to 10 iterations (11 minutes) to limit the discomfort to the participant, with a rest period offered between each test. Various measures had been taken to guarantee the safety of human participants. The amplitude and frequency of robot movement were set low to emulate the rehabilitation use for patients. Movement ability of each recruited participant would be assessed first before any tests. Emergency stops had also been designed from both hardware and software aspects.

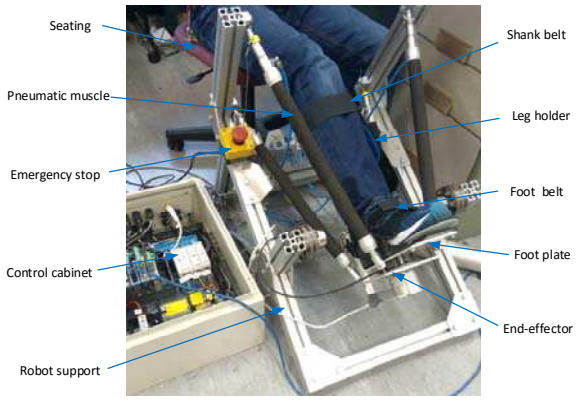

Fig. 5. Configuration of the robot experimental setup with human ankle.

Three tests were performed to validate the effectiveness of the multiple DOFs NIFT in different situations. In test 1 (T1), test 2 (T2), and test 3 (T3), the robot was controlled without human participants, with human passive, and human passive-then-active training, respectively. For T3, the participant was asked to actively move after 5 iterations of passive training to emulate the scenario where patients are making progress in their range of motion ability through rehabilitation, in order to explore how NIFT could adapt to the changing capabilities of the patient over time. To demonstrate the changes of operating conditions, the robot force/torque was recorded during each test. We take participant 1 as an example with results shown in Fig. 6 (a)-(d). For T3 the first 360 seconds indicate the passive iterations without user active forces, followed by 300 seconds with participant active interaction, where we can see that the participant exerted a distinctly higher force and torque starting from the 6th iteration. The end-effector orientation results under these three experiment conditions (T1, T2, T3) are shown in Fig. 6 (e). It can be seen at the end of tuning performances of T1, T2 and T3 were all satisfactory, even different ankle effects existed. The errors at the end of tuning (Fig. 6 (f)) were very similar in shape and magnitude.

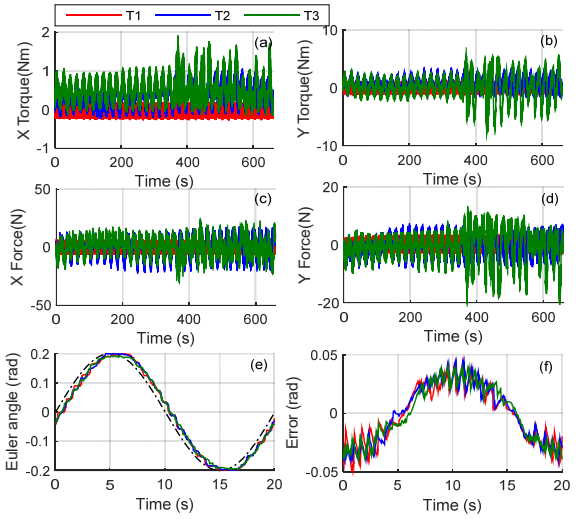

Fig. 6. Experimental results of T1, T2 and T3 with participant 1. (a) Interaction torques about X axis and (b) about Y. (c) Interaction forces along X axis and (d) along Y. (e) End-effector orientation results at the end of tuning. (f) End-effector orientation errors at the end of tuning.

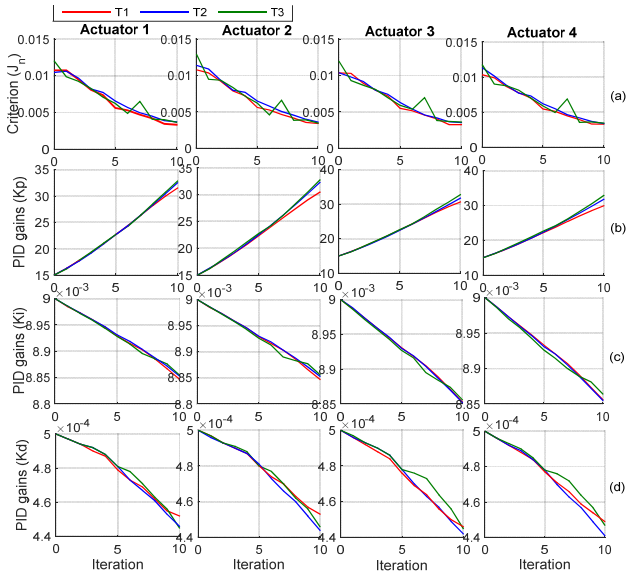

Fig. 7. Comparison of design criterion profiles and controller parameters K_P, K_I, and K_D for all actuators between T1, T2 and T3 with participant 1.

The NIFT's adaption to human affects can be examined by comparing the normalised design criterion values $J_n(\rho)$ during the three tests, with results shown in Fig. 7. There was a significant decline of the design criterion. It can be seen that $J_n(\rho)$ of no human participant test (T1) and human passive test (T2) were quite similar. For human participant passive-active test (T3), $J_n(\rho)$ for the all actuators stopped improving when the user started to actively move from the 6th iteration, due to a sudden disturbance applied to the robot by the participant. However, the NIFT method was able to adjust for this discrepancy immediately by tuning the controller gains to tackle external changes. It can be seen that the design criterion $J_n(\rho)$ started improving again after 2 iterations. The starting

error for T2 and T3 was higher than that of T1, due to the influence of human effects, but the control performance at the end of tuning were all satisfactory. The controller parameters in Fig. 7 can be examined to see the effect of NIFT tuning process. The value of K_P in T2 and T3 was higher than that in T1, because the human ankle would exert a resistance torque to the robot, so the controller had to increase the input value to keep tacking the predefined trajectory. The rate of change of K_P, K_I and K_D in T3 was tuned by NIFT to adapt to the human activities. Online tuning of the parameters made the controller achieve a high performance soon after external condition changes. It is also found that the controller parameters reached by each NIFT algorithm were different from one another due to misalignments for each actuator. It also provides evidence that each IFT algorithm was able to optimise its actuator properly in a multiple degrees-of-freedom implementation.

The NIFT was then experimentally compared against the standard IFT implementation based on T3 to demonstrate its improved robustness. The comparison of IFT and NIFT at iteration set ρ_5 and ρ_{10} in terms of parameter updating and control performance is shown in Fig. 8. It is evident that the rate of change of PID gains of IFT and NIFT were similar before ρ_5, while the differences became significant for all actuators after the user started active input. The rate of change of K_P of NIFT was significantly higher than that of IFT as the former can adapt to the operation changes in a faster way. The end-effector error of NIFT at 5th and 10th iteration was also smaller than that of IFT. These indicate that both IFT algorithms possess the robustness property to adapt to external changes, while the NIFT shows a better performance.

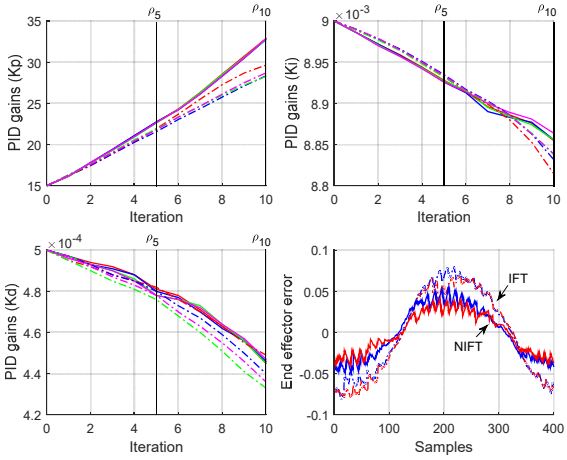

Fig. 8. Robustness test by comparison with standard IFT at ρ_5 and ρ_{10}: solid lines indicate the result of NIFT while dashed lines the IFT; red, blue, green and magenta lines represent the results of actuator 1 to 4, respectively.

To further verify the normalised IFT controller's robustness and adaptability, another three participants were recruited to perform the passive-active experiment with same procedure as described above to emulate changing of recovery stages. Similar findings can be concluded, as the NIFT instances increased the controller gains at a faster rate to compensate for the increase in ankle stiffness. The normalised design criterion values $J_n(\rho)$ of each participant are demonstrated in Fig. 9. The results show that the NIFT technique was able to adapt to the changing capabilities of different participants over time. Though the tracking performance for each participant was different especially when human effects existed, all controllers were able to track the reference trajectory better and better based on NIFT learning capacity and reached an ideal result within several minutes. Table II shows more statistical details to indicate the robustness of NIFT scheme for its adaptability to different participants with varying capabilities.

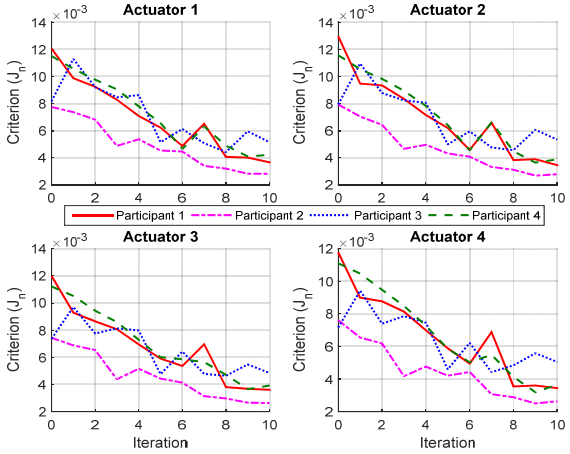

Fig. 9. Criterion profiles for passive-active tests across four participants.

To demonstrate the NIFT method's convergence property, an experiment with 20 iterations was conducted with results shown in Fig. 10. It is clear the NIFT successfully converged to a local optimum within 20 loops. The reason why we only applied 10 iterations in above tests is that it can reach a relatively good performance after 10 iterations and the next 10 did not result in significantly better results. Also a long time training may make the subjects uncomfortable and loss of patience. In this 20-iteration case, it took the algorithm until the 13th iteration to produce optimal results. The criterions and tuning process of PID gains of all actuators were plotted to indicate the convergence of NIFT method. From experiments throughout this research, the convergence speed of the NIFT technique was usually rapid, often within 10 to 20 iterations.

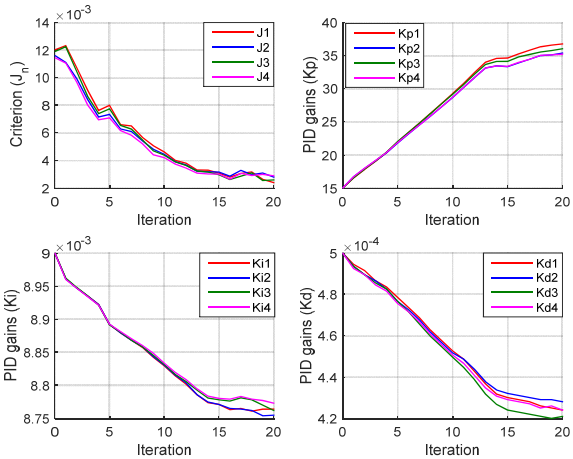

Fig. 10. Convergence test through a case study with 20 iterations: red, blue, green and magenta lines represent the design criterions and PID gains of actuator 1 to 4 of the ankle rehabilitation robot, respectively.

V. Discussion

Robotic rehabilitation devices can alleviate the manual therapy problems in terms of labour intensiveness, precision and subjectivity. Rehabilitation devices should be compliant to prevent discomforts and re-injuries during treatment. Different from most ankle rehabilitation robots that are driven by stiff actuators, the robot in this paper is intrinsically compliant due to the utilisation of PMAs. Repetitive training can contribute significantly to the effectiveness of treatment, it is crucial to design a robust robot controller to enable high performance repetitive ankle training for a long time. However, most of the current rehabilitation devices have some form of simple tuning control [26] that has to be manually adjusted to suit different capabilities of the patients. This research investigated the use of advanced iterative learning algorithm which has potential to provide advantages of high adaptability and robustness.

IFT technique is able to learn from repeating scenarios and to tune the controller parameters without knowledge of the actual system, which makes it suitable for repetitive control of a compliant robot driven by PMAs whose model is difficult to obtain. However, in order for the IFT to be used in real-life rehabilitation applications their robust performance must be guaranteed for a long time repetitive control. To the authors' knowledge no IFT control performance has been tested before in a rehabilitation robot. Though some papers [24, 37] applied IFT in rehabilitation, only the system output is adjusted based on previous data without considering the robust performance. In this paper, the performance of IFT is measured on a variety of operation conditions and different human participants to show that indeed the IFT technique can provide more control robustness to the rehabilitation robot, and is able to optimise the controller parameters for different situations encountered.

Previously, the weighting factor λ is determined by trial and error, which requires the designer to be experienced or to have an intimate knowledge of the system being tuned. In this paper, a normalised version of IFT controller was proposed to improve the robustness of the overall tuning technique and a multi-DOF NIFT implementation was conducted and tested on a compliant rehabilitation robot. To facilitate the comparison between above different tests, the RMS of the error value in each Euler direction and the maximum absolute error as well as the peak amplitude error in X direction are calculated. The resultant error values achieved from the standard IFT and normalised IFT tests are shown in Table I. The end-effector orientation errors are compared between the baseline (initial ZN tuned controller) and the IFT optimised controller (end of tuning) within a period of control (20s). It can be seen that the end-effector tracking performances at end of tuning for all IFT instances were significantly improved from the initial ZN performance. The maximum tracking errors in Euler X direction were kept to below 0.05 radians after IFT tuning. For standard IFT tests, the λ value of 1×10^{-3} was not optimal and with the gradual adjustment of λ to 1×10^{-4} and 1×10^{-5}, the error became smaller. The robustness for normalised IFT is better as it presented a better tracking performance than standard IFT tuned without changing λ_n.

Regarding the comparison between IFT and classical auto-tuning algorithms, there have been quite a few studies. Lequin et al. compared the performance of IFT-tuned PID controllers with the performance achieved by three other classical PID tuning schemes [34]. Tests in [21] showed the IFT can achieve up to 92% better performance compared to a conventional tuned controller. Hjalmarsson et al. also stated that the IFT method can obtain a faster response than other model-free methods [29]. The IFT algorithm has been verified to achieve a performance that is dramatically better than that of the classical PID tuning schemes. However, none of the research is conducted on the rehabilitation robots. This paper presents the comparison between NIFT method and the simple tuning algorithm on the compliant rehabilitation robot for the first time. Inspired by [21], the initial PID gains here were also obtained by using ZN rules and then the NIFT method started tuning from the ZN-tuned parameters to allow a direct comparison between them. From the tests it is shown that the IFT method always outperformed the initial ZN tuned approach, and the peak amplitude performance can reach up to 95.6% better performance than the ZN tuned sets. The NIFT showed improved robustness to different tests as compared to the standard IFT and the ZN rules that are commonly used.

The quantitative results with human participant experiments are demonstrated in Table II. The active joint torque applied to the system had a significant effect on the controller as well as the amplitude reached, especially in the X direction. For participant 1 the maximum amplitude that robot can reach decreased by 0.0077 and 0.0046 radians in dorsiflexion and plantarflexion direction, as the participant's ankle stiffness had resisted the robot movement. For the active input tests with four participants, the proposed normalised IFT algorithm instances

TABLE I
Quantitative comparison of standard and normalised IFT results

Test instances	Euler angle RMS error (rad)			Peak amplitude error (rad)		Max error (rad)
	X	Y	Z	Upper (X)	Lower (X)	X
Baseline (ZN tuning)	0.0626	0.0062	0.0255	0.0111	0.0114	0.1025
Standard IFT 1 $\boldsymbol{\lambda = 1 \times 10^{-3}}$	0.0510	0.0020	0.0075	0.0086	0.0063	0.0798
Standard IFT 2 $\boldsymbol{\lambda = 1 \times 10^{-4}}$	0.0316	0.0010	0.0011	0.0060	0.0029	0.0526
Standard IFT 3 $\boldsymbol{\lambda = 1 \times 10^{-5}}$	0.0242	0.0015	0.0010	0.0026	0.0012	0.0465
Normalised IFT $\boldsymbol{\lambda_n = 1 \times 10^{-4}}$	0.0239	0.0012	0.0010	0.0009	0.0005	0.0447

TABLE II
QUANTITATIVE COMPARISON OF IFT RESULTS WITH FOUR HUMAN PARTICIPANTS

Test instances	Participant details	Euler angle RMS error (rad)			Peak amplitude error (rad)	
		X	Y	Z	Upper (X)	Lower (X)
Normalised IFT test without human participant	Not applicable	0.0236	0.0015	0.0010	0.0008	0.0010
Passive test with human participant 1	Male, 1.70m, 61kg	0.0244	0.0017	0.0013	0.0009	0.0012
Passive-active test with human participant 1	Male, 1.70m, 61kg	0.0246	0.0018	0.0013	0.0077	0.0046
Passive-active test with human participant 2	Female, 1.65m, 52kg	0.0215	0.0016	0.0011	0.0065	0.0041
Passive-active test with human participant 3	Male, 1.78m, 75kg	0.0290	0.0019	0.0016	0.0086	0.0052
Passive-active test with human participant 4	Male, 1.73m, 67kg	0.0252	0.0011	0.0022	0.0077	0.0067

were able to successfully adapt to the changing users and capabilities. Considering the participant's active interaction as external noise to the robot, this finding is in accordance with [34]. We verified that the IFT method was able to take the noise disturbances into account and adjust the PID parameters to different values under noise or noise-free conditions. Similar findings can be concluded from Table II, as the NIFT algorithm increased the controller K_P gains to compensate for the increase in human ankle torque, the final tracking results were guaranteed in high-performance. Overall, it is concluded that the NIFT technique is robust, maintains system agnostic, and can be used to automatically adjust the robot controller to various operating conditions.

VI. CONCLUSION

This paper developed a robust control technique for repetitive control of robotic rehabilitation devices. A multiple degrees-of-freedom implementation of the normalised IFT technique was proposed and tested on a PMAs-actuated parallel ankle rehabilitation robot. The performance of this newly introduced normalised design criterion was put to the test against the commonly used standard IFT design criterion. Finally, four healthy human participants were recruited to validate the usage of NIFT on the ankle rehabilitation robot, as well as to validate the robustness and convergence efficacy of the proposed normalised IFT scheme. It can be concluded that the normalised IFT scheme provides robustness to the control system by adapting to different situations, which can in turn improves the effectiveness of robotic rehabilitation.

Future work can be done on the parallel ankle rehabilitation robot to further enhance the performance of iterative learning control. The performance of IFT technique depends on several factors, one of which being the optimisation algorithm. Apart from the Gauss-Newton algorithm presented in this paper, other optimisation algorithms can also be used, such as the Levenberg-Marquardt (LM) algorithm. No comparative study on these algorithms has been reported. On the other hand, advanced control schemes on the rehabilitation robot such as interaction control should also be examined to provide a more intuitive approach for robotic rehabilitation. Active control of the compliant robots can be approached by proper impedance control or adjustment of nominal pressure inside PMAs. Based on the measurement of patient's active contribution during training, the ILC method can be used to update the assistance accordingly by altering its weighting factor, which provides a promising way for assist-as-needed implementation.

NOMENCLATURE

H	Distance between the fixed and moving platforms
L_i	Vector representation of the i^{th} PMA link
O_f	Centre of fixed coordinate frame of the robot
O_m	Centre of moving coordinate frame of the robot
p_i^f	i^{th} connection point on the fixed platform
p_i^m	i^{th} connection point on the moving platform
R_m^f	Rotational matrix of the end-effector
$\theta_X, \theta_Y, \theta_Z$	Angular displacement of the end-effector
$C(\rho)$	Controller in 2-DOF form $C(\rho) = [C_r(\rho),\ C_y(\rho)]$
$J(\rho)$	Design criterion for IFT method
$J_n(\rho)$	Normalised design criterion for NIFT method
K_P, K_I, K_D	Parameters of basic PID controller to be tuned
K_n	Normalising coefficient
R_i	Gauss-Newton Hessian matrix
$R_{n,i}$	Normalised Gauss-Newton Hessian matrix
T_0, S_0	Temporary variables: $T_0 = \frac{C_r(\rho)G}{1+C_y(\rho)G},\ S_0 = \frac{1}{1+C_y(\rho)G}$
r_t	Reference input of the controlled system
$u_t(\rho)$	IFT controller input when parameter vector is ρ
v_t	Unmeasurable disturbance of the controlled system
$y_t(\rho)$	IFT controller output when parameter vector is ρ
$\tilde{y}_t(\rho)$	Error between the actual and the desired output
λ	Weighting factor of the design criterion
λ_n	Normalised weighting factor of the design criterion
ρ	Vector of PID parameters, $\rho = [K_P \quad K_I \quad K_D]^T$
γ_i	Step size for parameters updating

ACKNOWLEDGMENT

This research is funded by the National Natural Science Foundation of China (No. 51675389 and No. 51475342), and the Faculty of Engineering Research Development Fund (No. 3625057) of The University of Auckland.

REFERENCES

[1] P. R. d. A. Ribeiro and S. R. Soekadar, "A mechatronic system for robot-mediated hand telerehabilitation," *IEEE/ASME Transactions on Mechatronics,* vol. 20, pp. 1753-1764, 2015.

[2] M. Zhang, T. C. Davies, and S. Q. Xie, "Effectiveness of robot-assisted therapy on ankle rehabilitation - A systematic review," *Journal of NeuroEngineering and Rehabilitation,* vol. 10, 2013.

[3] W. Meng, Q. Liu, Z. Zhou, Q. Ai, B. Sheng, and S. Q. Xie, "Recent development of mechanisms and control strategies for robot-assisted lower limb rehabilitation," *Mechatronics,* vol. 31, pp. 132-145, 2015.

[4] M. Girone, G. Burdea, M. Bouzit, V. Popescu, and J. E. Deutsch, "A Stewart platform-based system for ankle telerehabilitation," *Autonomous Robots,* vol. 10, pp. 203-212, 2001.

[5] J. Saglia, N. Tsagarakis, J. S. Dai, et al., "Control strategies for patient-assisted training using the ankle rehabilitation robot (ARBOT)," *IEEE/ ASME Transactions on Mechatronics,* vol. 18, pp. 1799-1808, 2013.

[6] A. McDaid, Y. H. Tsoi, and S. Q. Xie, "MIMO actuator force control of a parallel robot for ankle rehabilitation," in *Interdisciplinary Mechatronics*, ed, 2013, pp. 163-208.

[7] A. U. Pehlivan, F. Sergi, and M. K. O'Malley, "A subject-adaptive controller for wrist robotic rehabilitation," *IEEE/ASME Transactions on Mechatronics,* vol. 20, pp. 1338-1350, 2015.

[8] P. K. Jamwal, S. Q. Xie, S. Hussain, and J. G. Parsons, "An adaptive wearable parallel robot for the treatment of ankle injuries," *IEEE/ASME Transactions on Mechatronics,* vol. 19, pp. 64-75, 2014.

[9] D. B. Reynolds, D. W. Repperger, C. A. Phillips, and G. Bandry, "Modeling the dynamic characteristics of pneumatic muscle," *Annals of Biomedical Engineering,* vol. 31, pp. 310-317, 2003.

[10] D. A. Bristow, M. Tharayil, and A. G. Alleyne, "A survey of iterative learning control," *IEEE Control Systems,* vol. 26, pp. 96-114, 2006.

[11] Z.-S. Hou and Z. Wang, "From model-based control to data-driven control: survey, classification and perspective," *Information Sciences,* vol. 235, pp. 3-35, 2013.

[12] G. Kwakkel, B. J. Kollen, and H. I. Krebs, "Effects of robot-assisted therapy on upper limb recovery after stroke: A systematic review," *Neurorehabilitation and Neural Repair,* vol. 22, pp. 111-121, 2008.

[13] S. Balasubramanian, R. Wei, M. Perez, B. Shepard, *et al.*, "RUPERT: An exoskeleton robot for assisting rehabilitation of arm functions," in *Virtual Rehabilitation*, 2008, pp. 163-167.

[14] C. Z. Lu, "Advanced Iterative Learning Algorithm for Control of Rehabilitation Robots," *The University of Auckland,* 2016.

[15] R. Chi, Z. Hou, S. Jin, D. Wang, and J. Hao, "A data-driven iterative feedback tuning approach of ALINEA for freeway traffic ramp metering with PARAMICS simulations,"*IEEE Transactions on Industrial Informatics,* vol. 9, pp. 2310-2317, 2013.

[16] H. Hjalmarsson, S. Gunnarsson, and M. Gevers, "A convergent iterative restricted complexity control design scheme," in *Proceedings of the 33rd IEEE Conference on Decision and Control*, 1994, pp. 1735-1740.

[17] H. Hjalmarsson, "Iterative feedback tuning—an overview," *International Journal of Adaptive Control and Signal Processing,* vol. 16, pp. 373-395, 2002.

[18] F. De Bruyne, "Iterative feedback tuning for internal model controllers," *Control Engineering Practice,* vol. 11, pp. 1043-1048, 2003.

[19] K. Hamamoto, T. Fukuda, and T. Sugie, "Iterative feedback tuning of controllers for a two-mass-spring system with friction," *Control Engineering Practice,* vol. 11, pp. 1061-1068, 2003.

[20] S. Kissling, P. Blanc, P. Myszkorowski, and I. Vaclavik, "Application of iterative feedback tuning (IFT) to speed and position control of a servo drive," *Control Engineering Practice,* vol. 17, pp. 834-840, 2009.

[21] A. J. McDaid, K. C. Aw, E. Haemmerle, and S. Q. Xie, "Control of IPMC actuators for microfluidics with adaptive “online” iterative feedback tuning," *IEEE/ASME Transactions on Mechatronics,* vol. 17, pp. 789-797, 2012.

[22] H.-S. Ahn, Y. Chen, and K. L. Moore, "Iterative learning control: brief survey and categorization," *IEEE Transactions on Systems Man and Cybernetics part C Applications and Reviews,* vol. 37, pp. 1099-1121, 2007.

[23] K. L. Meadmore, A.-M. Hughes, C. T. Freeman, Z. Cai, D. Tong, J. H. Burridge, *et al.*, "Functional electrical stimulation mediated by iterative learning control and 3D robotics reduces motor impairment in chronic stroke," *Journal of NeuroEngineering and Rehabilitation,* vol. 9, 2012.

[24] C. T. Freeman, E. Rogers, A.-M. Hughes, J. H. Burridge, and K. L. Meadmore, "Iterative learning control in health care: electrical stimulation and robotic-assisted upper-limb stroke rehabilitation," *IEEE Control Systems,* vol. 32, pp. 18-43, 2012.

[25] A. Duschau-Wicke, J. Von Zitzewitz, R. Banz, and R. Riener, "Iterative learning synchronization of robotic rehabilitation tasks," in *IEEE 10th International Conference on Rehabilitation Robotics, ICORR 2007*, 2007, pp. 335-340.

[26] S. Hussain, S. Q. Xie, and P. K. Jamwal, "Robust nonlinear control of an intrinsically compliant robotic gait training orthosis," *IEEE Transactions on Systems, Man, and Cybernetics: Systems,* vol. 43, pp. 655-665, 2013.

[27] G. Xu, A. Song, and H. Li, "Adaptive impedance control for upper-limb rehabilitation robot using evolutionary dynamic recurrent fuzzy neural network," *Journal of Intelligent & Robotic Systems,* vol. 62, pp. 501-525, 2011.

[28] M. F. Heertjes, B. Van der Velden, T. Oomen, "Constrained iterative feedback tuning for robust control of a wafer stage system," *IEEE Transactions on Control Systems Technology*, vol. 24, pp. 56-66, 2015.

[29] H. Hjalmarsson, M. Gevers, S. Gunnarsson, and O. Lequin, "Iterative feedback tuning: theory and applications," *IEEE Control Systems,* vol. 18, pp. 26-41, 1998.

[30] K. Kora, C. Z. Lu, and A. J. McDaid, "Automatic tuning with feedforward compensation of the HuREx rehabilitation system," in *2014 IEEE/ASME International Conference on Advanced Intelligent Mechatronics (AIM)*, 2014, pp. 1504-1509.

[31] J. K. Huusom, N. K. Poulsen, and S. B. Jørgensen, "Improving convergence of iterative feedback tuning," *Journal of Process Control,* vol. 19, pp. 570-578, 2009.

[32] C. Z. Lu, S. Q. Xie, and C. Deng, "Optimal normalized weighting factor in iterative feedback tuning of step input responses," in *IFAC Proceedings Volumes,* vol. 47, 2014, pp. 4790-4795.

[33] M.-B. Radac, R.-E. Precup, E. M. Petriu, S. Preitl, and C.-A. Dragos, "Data-driven reference trajectory tracking algorithm and experimental validation," *IEEE Transactions on Industrial Informatics,* vol. 9, pp. 2327-2336, 2013.

[34] O. Lequin, M. Gevers, M. Mossberg, E. Bosmans, and et al., "Iterative feedback tuning of PID parameters: comparison with classical tuning rules," *Control Engineering Practice,* vol. 11, pp. 1023-1033, 2003.

[35] M. Zhang, T. C. Davies, A. Nandakumar, and S. Q. Xie, "A novel assessment technique for measuring ankle orientation and stiffness," *Journal of Biomechanics,* vol. 48, pp. 3527-3529, 2015.

[36] M. Zhang, W. Meng, C. Davies, Y. Zhang, and S. Q. Xie, "A robot-driven computational model for estimating passive ankle torque with subject-specific adaptation," *IEEE Transactions on Biomedical Engineering,* vol. 63, pp. 814-821, 2015.

[37] L. Zhou, W. Meng, C. Z. Lu, Q. Liu, and S. Q. Xie., "Bio-inspired design and iterative feedback tuning control of a wearable ankle rehabilitation robot." *Journal of Computing and Information Science in Engineering*, doi:10.1115/1.4033900, in press, 2016.

Wei Meng received his M. Eng. degree from Wuhan University of Technology, China in 2013. From 2012 to 2016, he is a Doctoral Scholar working towards the joint PhD. degree in Wuhan University of Technology and the University of Auckland, New Zealand. He has directed two research projects and participated in over five research projects in areas of rehabilitation robots and interaction control. Wei Meng is the author of over 25 academic journal and conference papers and hold two patents. His research interests include robot-assisted rehabilitation, human-robot interaction and iterative learning control. He is an Editor of Cogent Engineering. Mr. Meng was a receipt of the Best Paper Award at the 2016 International Conference on Innovative Design and Manufacturing.

Sheng Q. Xie (SM’11) received his Ph.D. degree from Huazhong University of Science and Technology, China and University of Canterbury, New Zealand, in 1998 and 2002, respectively. In 2003, he joined The University of Auckland, where he is currently a Chair Professor in (bio)mechatronics. He has published 5 books, 15 book chapters, and over 280 international journal and conference papers. His current research interests are medical and rehabilitation robots, advanced robot control. Prof. Xie was elected a Fellow of The Institution of Professional Engineers

New Zealand (FIPENZ) in 2016. He has also served as a Technical Editor for IEEE/ASME TRANSACITONS ON MECHARTEONICS.

Quan Liu received her Ph.D. degree in 2003 from Wuhan University of Technology, China, where she is currently a Professor. During the recent five years, she authored over 60 technical publications, proceedings, editorials, and books. She has directed more than 20 research projects. Her research interests include signal processing, embedded systems, robots and electronics. She obtained 2 national awards and 3 provincial and ministerial awards. Prof. Liu was awarded as the "National Excellent Teacher" in 2007. She is the Council Member of Chinese Association of Electromagnetic Compatibility and the Hubei Institute of Electronics.

Charles Z. Lu received his Bachelor of Commerce and Bachelor of Engineering (1st Class Hons) degrees from University of Auckland, New Zealand in 2010. He then received his PhD in Mechanical Engineering in 2016 from the University of Auckland, researching rehabilitation robots and controller optimisation algorithms. He is currently working at a multinational Medical Devices company in Australia.

Qingsong Ai received his M.S. and Ph.D. degrees from Wuhan University of Technology, China, in 2006 and 2008, respectively. From 2006 to 2007, he was a visiting researcher at the University of Auckland, New Zealand, where he worked on medical robots. He is currently a Professor at the Wuhan University of Technology, and a senior editor of Cogent Engineering. Prof. Ai is the author of over 50 technical publications, proceedings, and editorials. In recent years, he has directed more than 10 research projects. His research interests include signal processing, rehabilitation robots and advanced manufacturing technology.